ADVANCED FUNCTIONAL MATERIALS
www.afm-journal.de

In Situ Damage Detection for Fiber-Reinforced Composites Using Integrated Zinc Oxide Nanowires

*LoriAnne Groo, Daniel J. Inman, and Henry A. Sodano**

A multifunction material that increases strength is capable of harvesting energy from ambient vibration and acts as a structural health monitoring system is presented. Current in situ damage detection of fiber-reinforced composites typically uses methods which require external sensors, precise initial measurements for each component under evaluation, or input current to the structure. To overcome these limitations, this work utilizes a multifunctional interphase of piezoelectric zinc oxide nanowires integrated into fiber-reinforced composites to provide an in situ ability to sense damage. The nanowires are grown onto insulating reinforcing fibers which are sandwiched between carbon fiber electrodes, thus fully integrating the sensing element into the fiber-reinforced composite. The fully distributed nanowire interphase proves capable of detecting multiple damage modes using passive voltage measurements as demonstrated during multiple loading configurations. This work also analyzes voltage emissions corresponding to damage to provide signal characteristics corresponding to the damage state of the specimen to indicate damage progression and the approach of catastrophic failure. The result of this work is thus a multifunctional structural material with damage detection capabilities. The principles investigated in this work can also be extended to alternative structural composites containing integrated piezoelectric materials in the form of nanoparticles, nanowires, or films.

1. Introduction

Fiber-reinforced composite materials are heavily used in modern marine, automobile, and aerospace structures due primarily to their high strength-to-weight ratio. However, due to the multiphase nature of the material and the critical nature of its applications, damage in the form of matrix cracking, fiber failure, fiber–matrix debonding, and interlaminar delamination can drastically affect the overall strength of the material leading to catastrophic failure. To detect this damage in its early stages, thus preserving the safety, reliability, and performance of the structure, substantial research efforts have been made in the fields of nondestructive evaluation (NDE) and structural health monitoring (SHM) which commonly use externally bonded piezoelectric sensors and transducers for in situ monitoring of structural components. The transducers are used to send and receive electronic signals to provide on-demand information regarding the functioning state of the composite structure without requiring the structure to be taken out of service thus leading to decreased maintenance costs and increased safety and reliability.[1–4] Two common methods for in situ damage detection for fiber-reinforced composites are acoustic emission testing (AET) and electrical resistance measurements. These methods are superior over alternative NDE methods in that they not only detect damage in situ, but recent developments have also demonstrated they can use embedded sensors thus eliminating the need for externally attached sensors and transducers.[5–12]

Traditional AET has been well established as an effective damage evaluation method using externally bonded piezoelectric and ultrasonic transducers.[13–15] Damage to the composite material in the form of debonding, crack initiation, or crack propagation results in a sudden release of energy leading to propagating elastic stress waves. Commercially available transducers detect the propagating stress waves at the surface of the material and send an electronic signal to the AET system and software for processing. Although effective in detecting damage, externally bonded sensors are exposed to environmental effects in addition to being limited by size, space, and surface state requirements. To overcome some of these challenges and aid the realization of AET for in-service composite structures, a variety of research has been completed in alternative sensors for AET with particular application in fiber-reinforced composites. For example, several groups have demonstrated the effectiveness of surface-bonded polyvinyledene fluoride (PVDF) sensors[16–19] and active fiber composites[20,21] in AET. These alternative sensors were shown to be capable of detecting the same damage as commercially available piezoelectric sensors without the rigidity and brittleness of traditional lead zirconate titanate wafers; however, the sensors still required external bonding to the structure under inspection. To more fully overcome limitations placed by external bonding, optical fibers as well as PVDF film sensors have been researched as fully embedded sensors in fiber-reinforced composites for AET.[5,6,22,23] In both cases, the fully

L. Groo, Prof. D. J. Inman, Prof. H. A. Sodano
Aerospace Engineering Department
1320 Beal Ave., Ann Arbor, MI 48109, USA
E-mail: hsodano@umich.edu
The ORCID identification number(s) for the author(s) of this article can be found under https://doi.org/10.1002/adfm.201802846.

DOI: 10.1002/adfm.201802846

embedded AET sensor was able to detect damage; however, the nature of the sensors used required predetermined positioning and discrete placement in the structure during the manufacturing process. They also provided no inherent structural benefit to the composite material and instead potentially increased the risk of debonding and delamination due to the inclusion of large diameter fibers or the inclusion of a fluorinated film which exhibits low surface energy for bonding. Thus, AET research up to this point has not led to an economical fully distributed sensor with inherent structural advantages.

In contrast to AET, damage detection via electrical impedance measurements utilizes the properties of the composite itself for damage sensing by applying a current to the test specimen and measuring the resulting voltage, thus calculating the sample resistance in situ. Several researchers have demonstrated the success of the method both for composite materials containing conductive fibers[7,8,12] and composites containing conductive fillers.[9–11] As the test specimen is subjected to mechanical loading, damage to the composite results in changes to the conductive pathways between the fibers or conductive fillers due to separation during debonding, delamination, or fiber cracking thus leading to changes in the electrical resistance of the test specimen.[7,8] The method is reliant on accurate initial resistance measurements as changes to this initial value are critical damage indicators. Among conductive fillers used for resistance measurements, carbon nanotubes are of particular interest. In addition to enabling in situ damage detection via resistance measurements for insulating fibers (i.e., glass fibers), successfully dispersed carbon nanotubes added to the reinforcing fibers or the supporting matrix have also been shown to increase the mechanical properties such as damping coefficient and interfacial shear strength of the host composite.[24–26] This increase in mechanical properties as well as accurate and reliable in situ damage detection consequently relies on the distribution of nanotubes, with the suggested distance between nanotubes being less than ≈1 nm for damage detection.[11,27,28] It follows that to achieve the required minimum separation careful synthesis and manufacturing techniques are necessary to prevent entangling or aggregation of the nanotubes while also ensuring adequate distribution and uniformity. The complexity of such techniques leads to concerns with ease of manufacturing, scalability, and widespread application of the studied deposition methods.[11,29,30] Additionally, damage detection via resistance measurements requires multiple electrode attachments as well as a constant current input resulting in demanding power requirements and system inefficiency when compared to a passive measurement. In contrast, the method presented in this work does not rely on any initial measurements of the test specimen and eliminates any current input by integrating piezoelectric nanowires into the structural composite itself as will be discussed further.

Zinc oxide (ZnO) nanowires have recently gained attention due primarily to their inherent piezoelectric and semiconducting properties as well as their contribution to the mechanical properties of the host composite.[31] ZnO nanowires can be grown directly onto woven or unidirectional fabric which is then integrated into fiber-reinforced composites using conventional manufacturing techniques. When included in this way, the nanowires form a functional interphase between the fiber and matrix. Multiple researchers have shown this tailorable fiber–matrix interphase results in increased tensile strength and modulus, increased interlaminar shear strength, and improved damping characteristics beyond those benefits reported from dispersed carbon nanotubes.[32–35] As previously mentioned, ZnO nanowires also possess both piezoelectric and semiconducting properties which enable actuation and sensing in addition to their appealing structural benefits. Prior work has utilized the piezoelectric coupling of the nanowires in energy harvesting by scavenging small amounts of power from ambient structural vibrations using flexible nanogenerators or fiber reinforced composites containing arrays of ZnO nanowires.[36–39] Additional work has also studied their use in a variety of sensors including humidity sensing,[40] chemical sensing,[41,42] and stress sensing.[43] However, although prior work has successfully applied structural and nonstructural functionalities of multifunctional composites containing ZnO, no other work to this point has demonstrated the use of the functional nanowire interphase for in situ damage detection.

This work utilizes a functional structural composite for self-sensing damage in situ using the described ZnO nanowire interphase. As damage occurs to the composite test specimen, the integrated nanowire interphase is strained resulting in a voltage emission from the nanowires due to the direct piezoelectric effect. The voltage across the test specimen is passively measured as the sample is mechanically loaded to detect such instances of voltage emission which indicate damage to the composite. In comparison to alternative in situ damage detection techniques such as AET or electrical resistance measurements, this method carries the added benefit of a completely distributed sensing material and conductive electrodes covering the entirety of the composite sample as well as the elimination of any reliance on initial measurements or input current requirements. The resulting functional composite is thus ideally suited for self-sensing minor damage over a large area or complicated structural components without requiring external sensors.

In this work, the nanowires were integrated into fiber-reinforced composites by directly growing them onto an insulating fabric which functions both as a reinforcing layer as well as the growth substrate. Conductive carbon fabric layers were then placed on the top and bottom of the insulating layer forming distributed electrodes as well as additional reinforcing layers. The resulting hybrid composites were then subjected to mechanical testing during which the voltage across the sample was measured for emissions corresponding to damage. Damage occurrence was also confirmed by use of a high-frequency microphone similar to traditional AET sensors. Finally, both the microphone and voltage measurements were analyzed to produce statistical damage metrics which can be used to track damage progression and predict the onset of catastrophic failure.

2. Results and Discussion

2.1. ZnO Synthesis and Composite Fabrication

ZnO nanowires were integrated into fiber-reinforced composites by conformally growing them on insulating plain weave

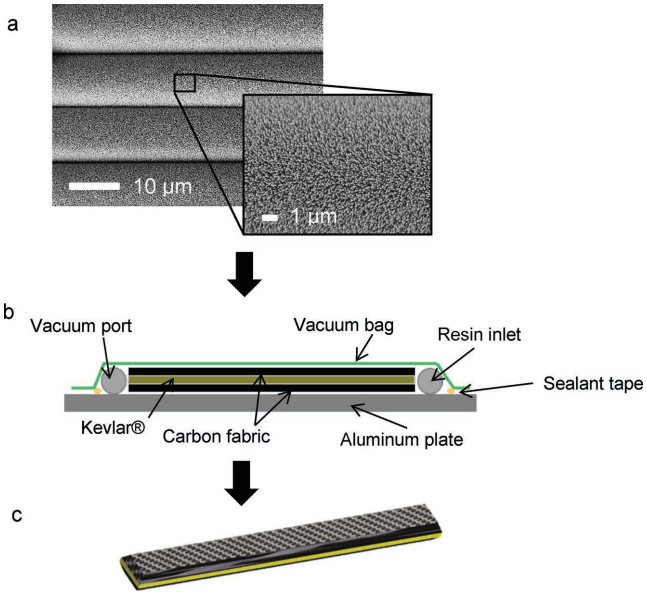

Figure 1. a) SEM image of ZnO nanowires on Kevlar, b) layup sequence of hybrid composite for VARTM, and c) test specimen cut from completed composite with polished edges.

aramid fabric using a two-step growth method that provides scalability. First, an initial seeding layer of ZnO nanoparticles was deposited onto the surface of the fabric through dip coating into a colloidal solution of quantum dots and thermally annealing the fabric. Following the nanoparticle deposition, the seeded fabric was placed into an aqueous growth solution in a convection oven for a low temperature hydrothermal growth. The resulting nanowire array conformally covered the entire surface of the aramid fabric as can be seen in the scanning electron microscope (SEM) image in **Figure 1**a. The fabric with ZnO nanowires was then sandwiched between layers of plain weave carbon fiber using vacuum-assisted resin transfer molding (VARTM) as depicted in Figure 1b. The outer layers of carbon fiber function as both conductive electrodes as well as reinforcing layers in the final composite. Neat samples fabricated from aramid fabric without nanowires and the same carbon fiber electrodes were also prepared using the same VARTM process to provide a baseline for comparison during all testing. Test coupons were then cut from the completed composites and the edges were polished to expose the insulating aramid fabric and eliminate shorting between the top and bottom electrodes as depicted in Figure 1c. Wire leads were then attached to each electrode using a combination of epoxy and conductive silver paint for voltage measurements during mechanical loading.

2.2. Three-Point Bend Testing

A standard three-point bend test was chosen to evaluate the completed composites' ability to self-sense the progression of matrix cracking, interfacial debonding, and potential fiber breakage occurring during flexural loading. The test was completed using an Instron load frame at a crosshead speed of 1 mm min^{-1}. In addition to the measurement of the applied load from the testing system, a high-frequency microphone was attached to the load frame close to the sample to detect damage via airborne acoustics similar to commercially available AET sensors. Air-borne acoustics have also independently been demonstrated to be an effective method for damage detection in previous works.[44] The voltage across the thickness of the test specimens was also simultaneously measured throughout all testing for any voltage emissions corresponding to the occurrence of damage. A schematic representation of the final test setup can be seen in **Figure 2**.

Several specimens were evaluated using the same testing setup. The load, specimen voltage, and microphone pressure reading all versus time for one functional composite containing piezoelectric ZnO nanowires are shown in **Figure 3**a through c, respectively. The figure clearly shows the progression of the test leading to the point of damage. Throughout the majority of the test, the microphone pressure reading as well as the voltage across the sample remains relatively constant around zero until the point where initial damage expected to occur in the form of matrix cracking is evident in all three measurements.

The final portion of the test duration during which measurable damage occurs is shown in Figure 3d through f at a larger scale for further evaluation. As additional matrix cracking and debonding in the composite occur, a corresponding change in the measured load, sample voltage, and microphone pressure can be observed. The detected emissions from both the microphone and the voltage reading show excellent coherence in both time of damage occurrence as well as the relative amplitude of the detected emissions, thus validating the ability of the voltage resulting from the ZnO to detect damage in situ during the test. Several works have conclusively established the use of AET sensors similar to the high-frequency microphone used in this work for detecting matrix cracking, interfacial debonding, and in some cases fiber breakage occurring during flexural loading; however, the classification of such damage using AET signal features such as amplitude distribution is complicated.[16,45] There

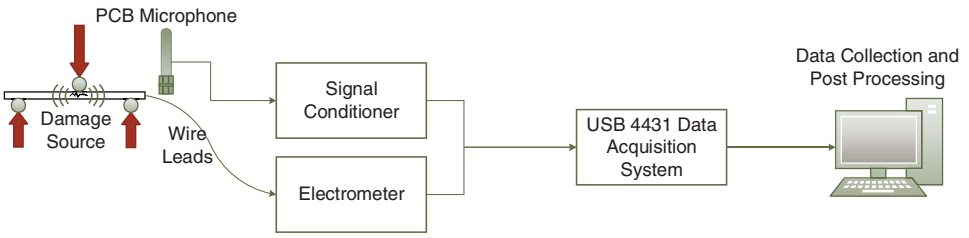

Figure 2. Schematic representation of three-point bend test setup.

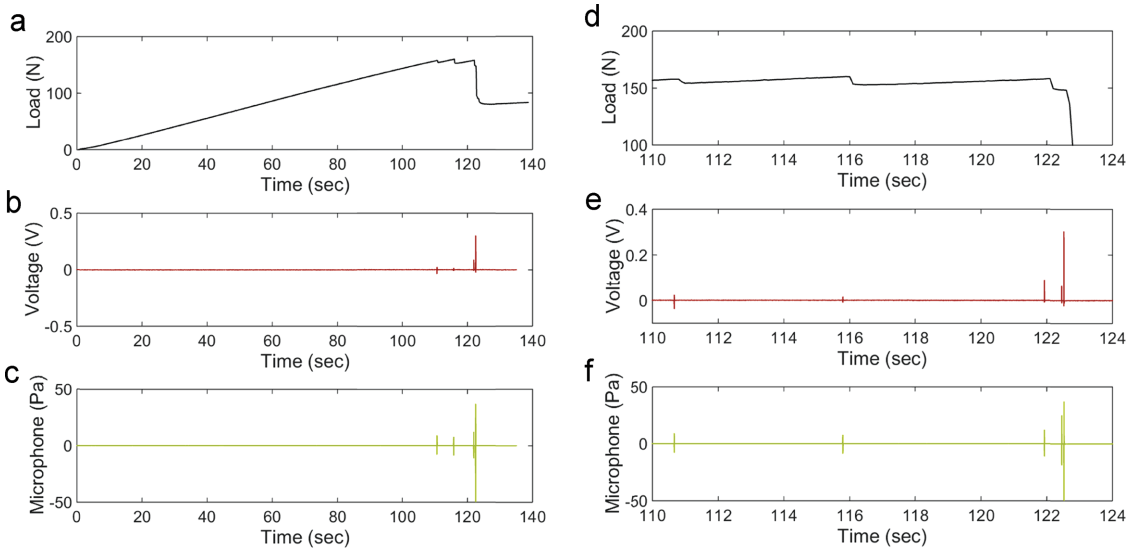

Figure 3. a) Applied load, b) measured voltage across sample, and c) microphone pressure reading during three-point bend test. Magnified section of d) applied load, e) measured voltage across sample, and f) microphone pressure reading during three-point bend test.

is, however, a general agreement in the correlation between increasing amplitude and damage severity indicating the early damage detected by both the microphone and voltage measurements likely corresponds to matrix cracking, while higher amplitude signals occurring later during testing are expected to correspond to interfacial debonding or fiber breakage. It should also be noted that while the microphone is capable of detecting the same damage to the composite, the voltage measurement has the significant advantage of complete integration into the structure and omnipresent distribution throughout the entirety of the sample. Additionally, the spontaneous charge separation resulting from damage due to the direct piezoelectric effect results in the same measurable voltage over the entire area of the test specimen. Thus, the high conductivity of the distributed carbon fiber electrodes ensures the voltage measurement can be made at any point over the specimen surface area, not just at the point of matrix or fiber failure which is promising for the scalability of the method to larger or more complicated structures.

To validate that it is in fact the piezoelectric nanowires responsible for indicating damage rather than other constituents, several baseline samples containing no ZnO nanowires were also tested using the same methodology and testing setup. The resulting load, test specimen voltage, and microphone pressure reading, all versus time for one baseline composite specimen can be seen in **Figure 4**a through c respectively. It is evident from the figure that the load measurement shows noticeable decreases in response to both matrix cracking as well as debonding and the microphone pressure shows corresponding measurements of acoustic emission. However, the voltage measurement across the bare sample remains relatively constant and shows little to no measureable change in response to the damage indicating the piezoelectric ZnO nanowire interphase is indeed required for passive damage detection.

The results from both the baseline and functional samples combine to establish the functionality of composites containing integrated ZnO nanowires in in situ damage detection. The voltage measurements indicate that the piezoelectric properties of the nanowires are responsible for detectable voltage emissions resulting from composite damage. Additionally, the time of occurrence of the emissions as well as the relative amplitude is in line with signals detected by the external microphone indicating variance in signal properties with damage severity. However, the type of damage the test specimen is exposed to in a three-point bend test is limited primarily to matrix cracking and some interfacial debonding; thus, further testing is required to fully characterize the role of ZnO nanowires for in situ damage detection during more extensive delamination and fiber failure.

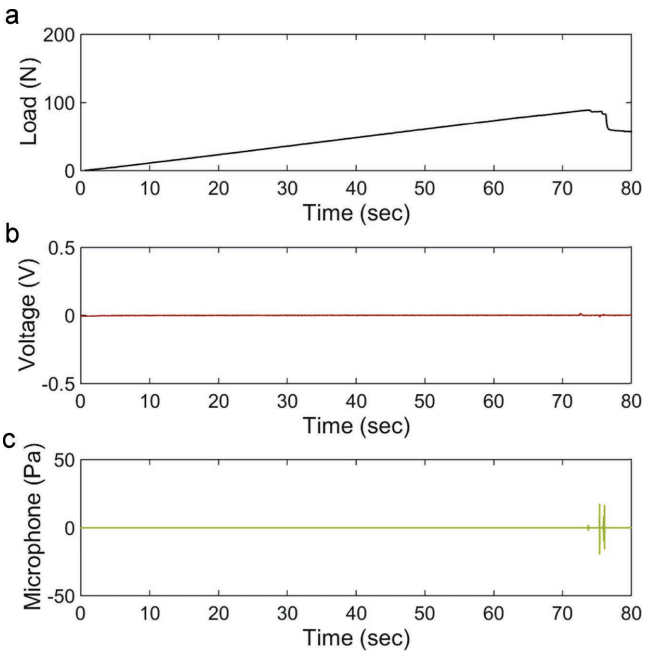

Figure 4. a) Applied load, b) voltage across test specimen, and c) microphone pressure reading during three-point bend test of baseline sample.

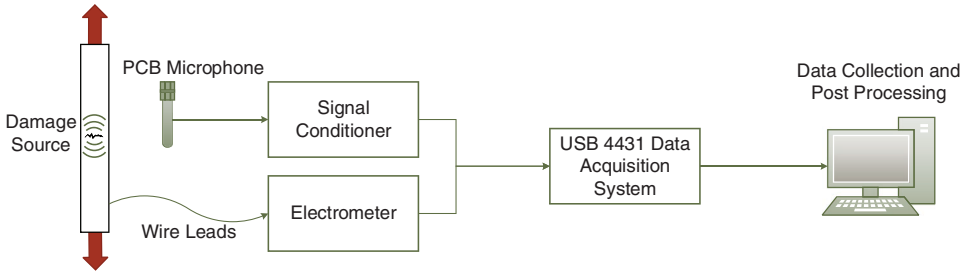

Figure 5. Schematic representation of tensile test setup.

2.3. Tensile Testing

To expand the information obtained from the three-point bend test, a standard composite tensile test was also completed for both samples containing ZnO nanowires as well as baseline samples without nanowires. The tests were completed using the same load frame again at a crosshead speed of 1 mm min^{-1}. In addition to further validating the detection of matrix cracking and interfacial debonding as seen during the three-point bend test, the tensile test also served to subject the test specimen to additional failure modes including fiber failure. Moreover, an increased number of emissions from both the microphone and voltage measurements were detected due to the nature of the applied load. As before, the voltage across the sample was measured and collected throughout the duration of the test as was the testing load and the microphone pressure as pictured in the test setup schematic representation is seen in **Figure 5**.

Due to the high value of the applied load during the tensile test, damage prior to catastrophic failure was not visible in the measured load as it was in the three-point bend test; however, the microphone was again used to detect air-borne acoustics resulting from matrix cracking, interfacial debonding, and fiber failure. As before, several samples were tested with each showing comparable results. A representative measured load, test specimen voltage, and microphone pressure reading are shown in **Figure 6**a through c, respectively.

Although the coherence between emission measurements from the voltage and acoustics detected by the microphone is not exact, good correlation is seen in the majority of the test duration indicating the nanowires are again capable of detecting the same composite damage as more conventional methods with the benefit of full integration. Additionally, the close correlation between measurements also confirms the functional composite is capable of detecting debonding or fiber breakage in both the reinforcing carbon fiber electrodes as well as the insulating aramid fabric with ZnO as damage to either material is detected via microphone measurements. For reference, a representative voltage and microphone reading for a single damage occurrence is also shown in Figure 6d through e, respectively.

A closer examination of the voltage emission during the tensile test as shown in Figure 6d,e provides additional insight regarding the damage detection mechanism of the sample containing integrated piezoelectric ZnO. Rather than detecting an acoustic burst-type pressure wave as is seen in the microphone reading, the composite sample instead acts as a capacitor which is initially charged as damage occurs and subsequently discharged. The rate of decay thus closely aligns with the expected theoretical rate calculated using the appropriate time constant for the sample's measured resistance and capacitance. The increase in measured voltage at the onset of the variety of damage types seen during testing is due to the inherent piezoelectricity of the individual nanowires which produce a corresponding charge as they are rapidly strained and mechanically perturbed. This charge was then detected via voltage output between the two external carbon fiber electrodes. The shape of

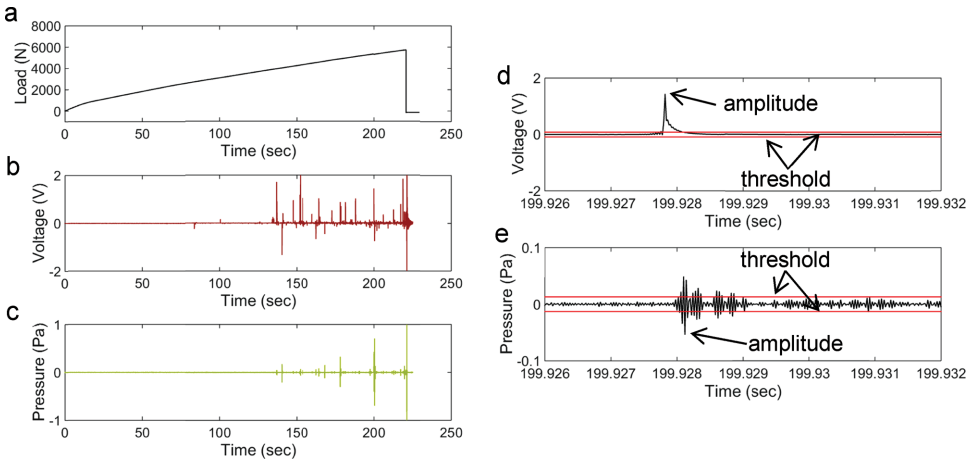

Figure 6. a) Measured testing load, b) voltage across test specimen, and c) microphone pressure reading during tensile test of sample containing ZnO nanowires. Magnified portion of d) voltage across test specimen and e) microphone pressure reading.

the signal seen in this work is not unexpected as it closely aligns with the measurements seen in other works studying the use of ZnO nanowires or nanorods in flexible nanogenerators.[46,47] Additionally, it should also be noted that the aramid fabric used as the insulating and reinforcing layer in the composite possesses a high damping coefficient which would also contribute to the signal's impulse and decay behavior as any internal vibratory oscillations resulting from damage are damped by the material itself. Thus, both the mechanism of damage detection as well as the substrate used for ZnO growth can be assumed to contribute to the characteristics of the measured signal, namely the impulsive charge followed by an immediate discharge.

The signal measurements of the test specimen voltage can be further evaluated to produce various signal characteristics based on traditional AET in order to provide additional damage progression information. A minimum voltage threshold above the baseline noise level of both the baseline samples and the samples containing ZnO was defined for both the voltage measurement and the microphone pressure reading. Any instance of the voltage crossing the selected threshold was then defined as a "hit." The maximum absolute value of the voltage throughout the hit duration was defined as the corresponding "hit amplitude." An example of the voltage hit, threshold, and amplitude of a voltage emission is shown in Figure 6d for clarity. As a basis for comparison, similar characteristics were also defined for the microphone burst signal as is seen in Figure 6e. In processing, each burst was defined as a single hit rather than counting each oscillation. Each hit was also required to be separated by 0.005 s to avoid recording echoes. To determine the threshold value, the root-mean-square (RMS) value of the baseline noise of both the voltage and microphone was initially calculated. An initial threshold was then selected for each data set and the RMS value of the detected hit amplitudes was calculated and divided by the RMS value of the baseline. The desired ratio of the RMS signal value to the RMS baseline noise was set to be within the range 1995–2005. The threshold was then iterated and the RMS value of the hit amplitudes was again calculated to determine the new signal-to-noise ratio. This process was repeated until the desired signal-to-noise ratio was achieved. The threshold was thus designed to account for variance in baseline noise between the voltage and microphone as well as variance in relative signal amplitude during a hit. In the case of the data set presented, the voltage threshold was set to 0.0875 V and the microphone threshold was set to 0.013 Pa, resulting in RMS signal-to-noise ratios of 1998.6 and 1996.7, respectively.

A scatterplot of the hit amplitude versus time during testing as well as the cumulative number of hits for both the test specimen voltage and the microphone pressure is shown in **Figure 7**a,b, respectively. The figure shows clear correlation between the damage detected using the developed functional composite and the established method using air-borne acoustics. In both figures, and most notably the figure representing the ZnO voltage measurements, the hit rate increases dramatically as the specimen approaches total failure. This indicates the nanowires alone can be used to predict the onset of catastrophic failure by monitoring the cumulative number of hits as well as the average time separation between hits. Additionally, the number of hits versus the hit amplitude for both the voltage measurement as well as the microphone reading for a single test is shown in Figure 7c,d, respectively. An analysis of both histograms, and most notably the ZnO voltage measurement, shows a higher number of hits at lower magnitude. This result follows a similar trend to that of data obtained using traditional AET sensors as well as established alternative sensors in prior works which have correlated the emission amplitude with damage severity.[16,45,48] Using the method established in this work, it can be inferred that the hit amplitude from the ZnO nanowires corresponds to the severity of the detected damage, i.e., more frequently occurring low-level damage such as matrix cracking corresponds to low-amplitude voltage emission, while fiber failure can be expected to correspond to higher-amplitude voltage emission. Although the nanowires follow similar trends indicating their potential use in classifying damage, it should also be noted that the integrated nature of the sensing nanowire interphase may result in damage to the nanowires as interfacial debonding and fiber failure occurs in the composite. This likely leads to a subtle decrease in the amplitude of the voltage output during such damage resulting in a larger overlap between

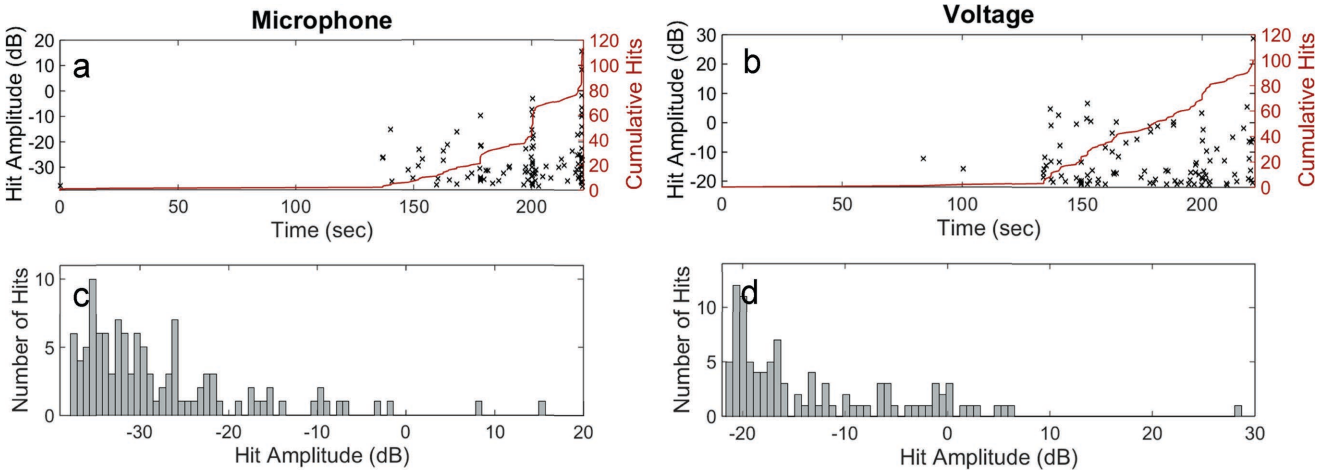

Figure 7. a) Scatter plot of hit amplitude versus time during test and cumulative hits versus time during test for microphone, b) scatter plot of hit amplitude versus time during test and cumulative hits versus time during test for test specimen voltage, c) histogram of hits versus amplitude for microphone reading, and d) histogram of hits versus amplitude for sample voltage.

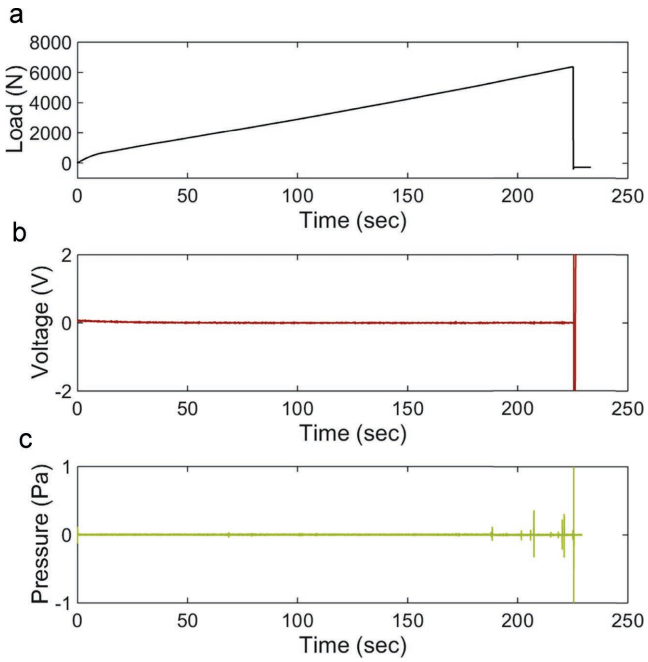

Figure 8. Measured testing load (top), voltage across test specimen (middle), and microphone pressure reading (bottom) during tensile test of baseline sample.

the amplitude distribution of matrix cracking with interfacial debonding and interfacial debonding with fiber breakage as the specimen approaches total failure. However, as previously stated, prior works have already established the difficult nature of classifying damage during in situ detection using alternative methods. Additionally, the benefit of the integrated and omnipresent ZnO nanowire sensing interphase in detecting early stage low-level damage outweighs any loss in amplitude detection when the sample is near catastrophic failure.

Finally, the sample containing neat Kevlar with no ZnO nanowires was also subjected to a tensile test to provide a baseline measurement. As anticipated, the sample showed no voltage emission corresponding to matrix cracking, interfacial debonding, or fiber failure throughout the duration of the test. The voltage measurement remained relatively constant around zero up to the point of catastrophic failure occurring in the middle of the sample, at which point the wire lead detached from the sample. The measured testing load from the load frame, the measured voltage, and the microphone pressure for one test specimen can all be seen in **Figure 8**a through c, respectively.

3. Conclusions

In this work, a multifunctional interphase of piezoelectric ZnO nanowires is utilized for damage sensing in a fiber-reinforced composite material. Both the sensing interphase and electrodes are comprised of structural materials and are fully distributed throughout the plane of the composite material allowing for the detection of minor damage in any location. Additionally, the same nanowire interphase used for damage detection in this work has been shown in previous research to contribute to the mechanical properties of the host composite as well as scavenge small amounts of power from ambient vibrations. Thus, this work further advances the multifunctional nature of composites containing ZnO nanowires by conclusively establishing the ability of integrated ZnO nanowires to detect damage in fiber-reinforced composites during both flexural and tensile loading and validating the damage detected using air-borne acoustics similar to AET. Matrix failure, interfacial debonding, delamination, and fiber failure within the test specimen containing ZnO was shown to result in a spontaneous charge separation that could be detected via voltage output and defined as a voltage emission. The voltage emission resulting from the piezoelectric properties of the nanowires was thus used to indicate the occurrence of damage, while the accumulation of such events indicated damage progression and the approach of catastrophic failure. Trends in both the distribution of hit amplitude as well as the rate of emissions during testing and the cumulative number of hits were shown to follow similar trends to those of traditional acoustic emission sensors; consequently, the performance of the nanowires is comparable to traditional acoustic emission sensors with the significant added benefit of full incorporation into the entirety of the composite structure. As a result, this work overcomes major hurdles in the widespread application of alternative in situ damage detection techniques by exploiting the ability of functional structural composites containing ZnO nanowires to self-sense damage.

4. Experimental Section

Fabric Preparation: Plain weave aramid fabric (Kevlar KM2+ Style 790, CS-800, 4.3 oz/yd^2, received from JPS Composite Materials) was selected as the ZnO nanowire growth substrate as well as the insulating layer in the final composite. The fabric was first prepared by cleaning and functionalization processes as outlined by Ehlert and Sodano.[49] The fabric was cleaned using subsequent washes of boiling acetone and boiling ethanol, after which it was dried under vacuum at 100 °C for 1 h. The cleaning process simply acted to remove any organic contaminants on the surface of the fabric. Following cleaning, the fabric was functionalized using a 10% aqueous solution of sodium hydroxide (Fisher Chemical, Certified ACS Pellets) at room temperature. The fabric was soaked in the solution at room temperature for 20 min after which it was rinsed thoroughly with deionized (DI) water and dried under vacuum at 100 °C for 1 h. The functionalization was followed by an ion exchange using 33% hydrochloric acid (Fisher Chemical, Certified ACS). The fabric was briefly dipped in the acid after which it was again thoroughly rinsed with DI water and dried following the same procedure.

ZnO Growth: A colloidal suspension method first outlined by Wong and Searson[50] was used to deposit an initial seeding layer of ZnO nanoparticles onto the surface of the Kevlar fabric. To prepare the nanoparticle solution, 0.0125 M concentrate of zinc acetate dihydrate (Sigma-Aldrich, >99%) and 0.02 M concentrate of sodium hydroxide were dissolved separately in ethanol at 50 and 60 °C respectively under vigorous stirring. Once the powders had been allowed to fully dissolve, 32 mL of the zinc acetate mixture was diluted with 256 mL ethanol, and 32 mL of the sodium hydroxide mixture was diluted with 80 mL of ethanol. Each solution was heated separately to 55 °C after which the sodium hydroxide/ethanol solution was added dropwise to the zinc acetate dehydrate in ethanol. The solution was allowed to mix at 55 °C for 45 min after which the nanoparticle growth was quenched using an ice bath.

The previously prepared fabric was dipped in the nanoparticle solution to deposit a seeding layer onto the surface of the fabric. After dipping in the colloidal suspension of nanoparticles, the seeding layer was annealed at 150 °C for 10 min and subsequently cooled for 10 min. This seeding, annealing, and cooling procedure was completed three times to ensure a uniform layer of nanoparticles fully covered the surface of the fabric. The fabric with ZnO nanoparticles was then submerged in a solution containing 0.075 M zinc nitrate hexahydrate (Sigma-Aldrich, >99%) and 0.075 M hexamethylenetetramine (Sigma-Aldrich, >99%) in DI water and the fabric and solution were placed in a convection oven at 80 °C for 8 h for nanowire growth. Following growth, the fabric was rinsed thoroughly in DI water and dried in the same convection oven for 1 h. The nanowires were then examined using a scanning electron microscope (JSM-7800F) as seen in Figure 1b.

Composite Fabrication: Functional hybrid composites were fabricated using the Kevlar with ZnO nanowires combined with plain weave carbon fabric (Hexcel HexForce Style SGP196-P, 5.80 oz/yd^2) to act as both structural reinforcement as well as electrodes. In the case of the three-point bend composites, two inner layers of Kevlar were used with one carbon fabric layer on both top and bottom; however, the tensile specimens contained only one layer of Kevlar. This was done to increase the thickness of the flexure samples for practicality of testing. The inner surfaces of the carbon fabric layers in contact with the ZnO nanowire interface were sputtered with gold to form a metal–semiconductor junction in order to create a Schottky barrier for improved sensing and actuation performance of the ZnO nanowire arrays.[36,51] A commercially available epoxy comprised of Epon 862 resin combined with curing agent Epikure 3230 (both received from Hexion) at a ratio of 100:35 was used as the composite matrix. The epoxy was distributed throughout each fabric layer using the VARTM method and cured following a curing cycle of 10 h at room temperature, followed by 2 h at 80 °C, and a 125 °C postcure for 3 h all under 100 psi (6.89 kPa) compression. Individual three-point bend samples were cut from the completed composite to meet ASTM D7264 standard sizes for composite testing; however, additional length was added to the specimens than is recommended for traditional three-point bend testing. This was done to ensure adequate space for the attachment of wire leads for voltage measurements. The completed three-point bend test specimens were 0.8 mm in thickness, 13 mm wide, and ≈100 mm long and were tested at a span ratio of 40:1. The tensile specimens were cut to dimensions of 100 mm in length and 10 mm in width per ASTM D3039 standards. After the samples were cut, the edges of both the tensile and three-point bend samples were polished to expose the insulating Kevlar layer and eliminate shorting between the top and bottom electrodes. Glass fabric tabs prepared using the same commercial epoxy matrix and VARTM technique were attached to the tensile samples using Loctite EA 9430 two-part adhesive and in coordination with ASTM D3039 standards. The outermost insulating epoxy layer was then removed to expose the carbon fabric in a small area of both the top and bottom surface of the three-point bend and tensile samples after which 33 gauge magnet wires were then attached to the exposed area using a combination of epoxy and silver paint for voltage measurements during testing. Baseline samples were prepared following the same methodology; however, untreated Kevlar with no ZnO was used as the insulating layer.

Experimental Setup: The completed samples were testing using an Instron 5969 load frame with a crosshead speed of 1 mm min^{-1}. The load frame was used to directly measure the applied load and the sample extension during testing. Throughout each test, a high-frequency microphone (PCB 426A05) and signal conditioner (PCB 482A16) were used to detect damage using air-borne acoustics. The microphone was attached to the testing frame as close as possible to the test specimen without interfering with the testing mechanisms. The voltage across baseline samples as well as samples containing ZnO was measured during testing using the previously attached wire leads which were connected to a Keysight B2985A electrometer. Both the microphone and voltage measurements were collected through the duration of each test using a National Instruments USB-4431 data acquisition system at a rate of 51.2 kHz. During data collection, the microphone pressure reading was also filtered using a 10 kHz high-pass second order Butterworth filter generated by an in-house LabVIEW program to reduce the amount of external noise. The voltage measurements did not receive any additional processing or preamplification.

Acknowledgements

This work was supported by a NASA Space Technology Research Fellowship and in part by the University of Michigan.

Conflict of Interest

The authors declare no conflict of interest.

Keywords

damage detection, fiber-reinforced composites, self-sensing, voltage emission, ZnO nanowires

Received: April 25, 2018
Revised: June 4, 2018
Published online: July 1, 2018

[1] A. Z. V. Giurgiutiu, J. Bao, *J. Intell. Mater. Syst. Struct.* **2004**, *15*, 673.
[2] X. Zhao, H. Gao, G. Zhang, B. Ayhan, F. Yan, C. Kwan, J. L. Rose, *Smart Mater. Struct.* **2007**, *16*, 1208.
[3] J. Yang, F.-K. Chang, *Smart Mater. Struct.* **2006**, *15*, 581.
[4] A. Cuc, V. Giurgiutiu, S. Joshi, Z. Tidwell, *AIAA J.* **2007**, *45*, 2838.
[5] P. F. Ian Read, Stuart Murray, *Meas. Sci. Technol.* **2002**, *13*, N5.
[6] C. Caneva, I. M. De Rosa, F. Sarasini, *Adv. Mater. Res.* **2006**, *13–14*, 337.
[7] J. C. Abry, S. Bochard, A. Chateauminois, M. Salvia, G. Giraud, *Compos. Sci. Technol.* **1999**, *59*, 925.
[8] J. Wen, Z. Xia, F. Choy, *Composites, Part B* **2011**, *42*, 77.
[9] E. T. Thostenson, T. W. Chou, *Nanotechnology* **2008**, *19*, 215713.
[10] N. D. Alexopoulos, C. Bartholome, P. Poulin, Z. Marioli-Riga, *Compos. Sci. Technol.* **2010**, *70*, 260.
[11] S.-l. Gao, R.-C. Zhuang, J. Zhang, J.-W. Liu, E. Mäder, *Adv. Funct. Mater.* **2010**, *20*, 1885.
[12] C. Baron, K. Schulte, *Materialpruefung* **1988**, *30*, 361.
[13] N. G. S. Huguet, R. Gaertner, L. Salmon, D. Villard, *Compos. Sci. Technol.* **2002**, *62*, 1433.
[14] A. C. M. Giordano, C. Esposito, A. D'Amore, L. Nicolais, *Compos. Sci. Technol.* **1998**, *58*, 1923.
[15] A. G. Kanji Ono, *J. Acoust. Emiss.* **2012**, *30*, 180.
[16] H. N. Bar, M. R. Bhat, C. R. L. Murthy, *J. Nondestr. Eval.* **2005**, *24*, 121.
[17] H. O. I. Narisawa, *J. Mater. Sci.* **1984**, *19*, 1777.
[18] H. O. I. Narisawa, *J. Mater. Sci.* **1985**, *20*, 4527.
[19] M. P. I. Grabec, *Sens. Actuators* **1984**, *5*, 275.
[20] M. Barbezat, A. J. Brunner, P. Flüeler, C. Huber, X. Kornmann, *Sens. Actuators, A* **2004**, *114*, 13.
[21] A. J. Brunner, M. Barbezat, P. Flüeler, C. Huber, *J. Acoust. Emiss.* **2004**, *22*, 127.
[22] I. M. D. R. C. Caneva, F. Sarasini, *Strain* **2008**, *44*, 308.
[23] I. M. De Rosa, F. Sarasini, *Polym. Test.* **2010**, *29*, 749.
[24] S. U. Khan, C. Y. Li, N. A. Siddiqui, J.-K. Kim, *Compos. Sci. Technol.* **2011**, *71*, 1486.
[25] J.-S. Jang, J. Varischetti, J. Suhr, *Carbon* **2012**, *50*, 4277.

[26] E. Thostenson, W. Li, D. Wang, Z. Ren, T. Chou, *J. Appl. Phys.* **2002**, *91*, 6034.
[27] I. Balberg, D. Azulay, D. Toker, O. Millo, *Int. J. Mod. Phys. B* **2004**, *18*, 2091.
[28] F. Du, R. C. Scogna, W. Zhou, S. Brand, J. E. Fischer, K. I. Winey, *Macromolecules* **2004**, *37*, 9048.
[29] Y. Zeng, L. Ci, B. J. Carey, R. Vajtai, P. M. Ajayan, *ACS Nano* **2010**, *4*, 6798.
[30] R. Sadeghian, S. Gangireddy, B. Minaie, K.-T. Hsiao, *Composites, Part A* **2006**, *37*, 1787.
[31] Z. L. Wang, *J. Phys.: Condens. Matter* **2004**, *16*, R829.
[32] U. Galan, Y. Lin, G. J. Ehlert, H. A. Sodano, *Compos. Sci. Technol.* **2011**, *71*, 946.
[33] M. H. Malakooti, H. S. Hwang, H. A. Sodano, *ACS Appl. Mater. Interfaces* **2015**, *7*, 332.
[34] H.-S. Hwang, M. H. Malakooti, H. A. Sodano, *Composites, Part A* **2015**, *76*, 326.
[35] A. Hazarika, B. K. Deka, D. Kim, K. Kong, Y.-B. Park, H. W. Park, *Composites, Part A* **2015**, *78*, 284.
[36] M. H. Malakooti, B. A. Patterson, H.-S. Hwang, H. A. Sodano, *Energy Environ. Sci.* **2016**, *9*, 634.
[37] A. Khan, M. Hussain, O. Nur, M. Willander, E. Broitman, *Phys. Status Solidi* **2015**, *212*, 579.
[38] T. S. van den Heever, W. J. Perold, *Smart Mater. Struct.* **2013**, *22*, 105029.
[39] J. S. Zhong Lin Wang, *Science* **2006**, *312*, 242.
[40] Y. Zhang, K. Yu, D. Jiang, Z. Zhu, H. Geng, L. Luo, *Appl. Surf. Sci.* **2005**, *242*, 212.
[41] R. K. Joshi, Q. Hu, F. Alvi, N. Joshi, A. Kumar, *J. Phys. Chem. C* **2009**, *113*, 16199.
[42] J. Zang, C. M. Li, X. Cui, J. Wang, X. Sun, H. Dong, C. Q. Sun, *Electroanalysis* **2007**, *19*, 1008.
[43] M. Villani, D. Delmonte, M. Culiolo, D. Calestani, N. Coppedè, M. Solzi, L. Marchini, R. Bercella, A. Zappettini, *J. Mater. Chem. A* **2016**, *4*, 10486.
[44] S. P. Thomas Krause, J. Ostermann, in *International Wind Engineering Conference*, Hannover, Germany **2014**.
[45] N. Chandarana, D. M. Sanchez, C. Soutis, M. Gresil, *Materials* **2017**, *10*, 685.
[46] G. Zhu, R. Yang, S. Wang, Z. L. Wang, *Nano Lett.* **2010**, *10*, 3151.
[47] Y. Qiu, H. Zhang, L. Hu, D. Yang, L. Wang, B. Wang, J. Ji, G. Liu, X. Liu, J. Lin, *Nanoscale* **2012**, *4*, 6568.
[48] M. Assarar, D. Scida, W. Zouari, E. H. Saidane, R. Ayad, *Polym. Compos.* **2016**, *37*, 1101.
[49] G. J. Ehlert, H. A. Sodano, *ACS Appl. Mater. Interfaces* **2009**, *1*, 1827.
[50] E. M. Wong, J. E. Bonevich, P. C. Searson, *J. Phys. Chem. B* **1998**, *102*, 7770.
[51] L. J. Brillson, Y. Lu, *J. Appl. Phys.* **2011**, *109*, 8.

